

# Effect of Hydrogen Addition on Softening and Melting Reduction Behaviors of Ferrous Burden in Gas-Injection Blast Furnace



YANA QIE, QING LYU, XIAOJIE LIU, JIANPEN LI, CHENCHEN LAN, SHUHUI ZHANG, and CHAOJIE YAN

The softening and melting reduction behaviors of ferrous burden in a gas-injection blast furnace (BF) have been investigated experimentally with the assistance of H<sub>2</sub>. The results indicate that the initial softening temperature of the burden in the BF is lower than that in the traditional BF, while the opposite trend is observed for its melting and dripping temperatures, thus widening the softening range and narrowing the melting zone. As a result, the permeability of the stock column is apparently improved, owing to the decreased amount of the produced melt. After H<sub>2</sub> gas is added, the thickness of the iron shell of the burden pellet increases, and the quantity of its liquid wüstite core decreases due to the higher reduction degree. The reduction rate of iron oxides is much faster than the carburization rate with the H<sub>2</sub> addition, and the dripping behavior of the ferrous burden is determined by the carburization with a high reduction potential. After taking into account the effects of H<sub>2</sub> addition on the iron oxide reduction rate, melt quantity, burden microstructure, and energy consumed by the gas-injection BF, it has been concluded that the optimal H<sub>2</sub> content lies in the range between 10 and 15 pct.

<https://doi.org/10.1007/s11663-018-1299-3>

© The Minerals, Metals & Materials Society and ASM International 2018

## I. INTRODUCTION

THE energy-intensive iron and steel industry is responsible for approximately 6.7 pct of the total anthropogenic CO<sub>2</sub> emissions across the world, according to the International Energy Agency.<sup>[1]</sup> The majority of these emissions (over 70 pct) are produced by iron-making blast furnaces (BFs), which also consume the largest amount of energy in the entire industry.<sup>[2]</sup> The traditional BF strongly relies on coke, which represents a large part of the production cost. Newly developed BF technologies focus on the utilization of various coke alternatives including natural gas, pulverized coal, plastic waste, biomass, coke oven gas, and other hydrocarbons.<sup>[3–12]</sup> However, the practical applicability of these materials strongly depends on the distribution of natural resources.<sup>[13]</sup> In addition, the top gas recycling blast furnace (TGR-BF) has attracted much attention in the recent decades due to its ability to

decrease both energy consumption and decrease the level of CO<sub>2</sub> emissions.<sup>[13,14]</sup> For example, top gas recycling and tuyère injection of oxygen were the primary methods used in the ULCOS project.<sup>[15]</sup> Nonetheless, the cost of CO<sub>2</sub> capture in the TGR-BF can be as high as \$56/tCO<sub>2</sub>.<sup>[16]</sup> Currently, pulverized coal injection (PCI) remains the main technique for decreasing the coke rate,<sup>[17]</sup> and the highest reported amount of injected coal is equal to approximately 250 kg/tHM (tons of hot metal), which is close to the amount of coke. However, the impact of the coal chemical properties must be also taken into account since they may prevent its complete combustion within the raceway, affect the gas permeability in the shaft, and contaminate the dead man zone, leading to irregular operation of the furnace and decreasing its productivity.<sup>[14,18]</sup>

The gas-injection BF is a new iron-making technology that allows injecting gas into tuyères and recycling the top gas through a gasifier, which serves as a new gas source and effectively converts CO<sub>2</sub> in the BF top gas into CO at a relatively low cost. As compared with the traditional BF with PCI, the gas-injection BF can potentially simplify the iron-making process and recycle the BF top gas, thus decreasing CO<sub>2</sub> emissions and increasing the furnace productivity. The utilized process consists of the following steps: BF top gas is injected into the gasifier as the gasifying agent → coal

YANA QIE, QING LYU, XIAOJIE LIU, JIANPEN LI, CHENCHEN LAN, SHUHUI ZHANG, and CHAOJIE YAN are with the College of Metallurgy & Energy, Key Laboratory for Advanced Metallurgy Technology, North China University of Science and Technology, Tangshan 063009, China. Contact e-mail: 461434073@qq.com

Manuscript submitted July 28, 2017.

Article published online June 25, 2018.

gasification occurs in the gasifier → H<sub>2</sub>-rich gas is produced → H<sub>2</sub>-rich gas is heated using the gas heating device → the high-temperature gas and hot air are injected into the furnace through the tuyères (Figure 1).

In addition, inferior coal of high-volatile can be utilized in the gas-making process, which not only decreases the dependence of BF smelting on high-quality coke,<sup>[19,20]</sup> but also increases the hydrogen content, thus improving the BF production efficiency.<sup>[21]</sup>

The meltdown of ferrous burden determines the inner shape of the BF cohesive zone and affects the permeability and distribution of its gaseous content.<sup>[22]</sup> Hence, various techniques have been developed to characterize the softening and melting parameters of ferrous burden. Nogueira and Fruehan<sup>[23,24]</sup> examined different stages of the softening and melting of ferrous feed materials processed inside the BF. They also analyzed the evolution of the burden microstructure above the softening temperature and possible interactions between different types of pellets. The obtained results revealed that, during the process of assimilation between different burdens, the exudation of liquid phases from acidic pellets represented the key step. Nishimura *et al.*<sup>[25]</sup> investigated the high-temperature properties of various types of raw materials and examined the viscosity dependence of their shrinking behavior. As a result, solid sinter was formed from FeO and gangue due to the increase in the reduction degree, which increased the melting start temperature. Sunahara *et al.*<sup>[26]</sup> analyzed the effect of coke reactivity on the softening and melting properties of sinter. They found that increasing the coke reactivity index lowered the gasification start temperature, which increased the sinter reduction rate at 900 °C

to 1000 °C and decreased the permeable resistance index in the high-temperature region. Matsumura *et al.*<sup>[27]</sup> examined the effect of chemical composition on the sinter softening properties and concluded that the sinter with low SiO<sub>2</sub> and CaO contents exhibited superior high-temperature characteristics due to the low fraction of CaO-FeO-SiO<sub>2</sub> melt, whereas the high MgO content enhanced its reducibility and softening properties. An *et al.*<sup>[28,29]</sup> studied the softening and melting behaviors of mixed burden processed in an oxygen BF and determined its degree of permeability. Yang *et al.*<sup>[30]</sup> simulated the softening and melting processes occurring in multiple burden layers using computational fluid dynamics and discrete element methods.

In the gas-injection BF, the softening and melting reduction characteristics of ferrous burden (representing the dominant factors affecting the permeability of the ore layer) strongly depend on the concentration of the utilized reducing gas (such as CO and H<sub>2</sub>). Therefore, in this study, the effects of hydrogen addition on the softening and melting reduction behaviors of ferrous burden were examined to determine the parameters of the cohesive zone of the gas-injection BF and optimal H<sub>2</sub> content.

## II. EXPERIMENTAL

The ferrous burden used in BF is generally composed of sinter, lump ore, and pellets. The softening and melting reduction processes of these iron-bearing components are relatively similar despite the different compositions and structures of various burdens.<sup>[22]</sup> In

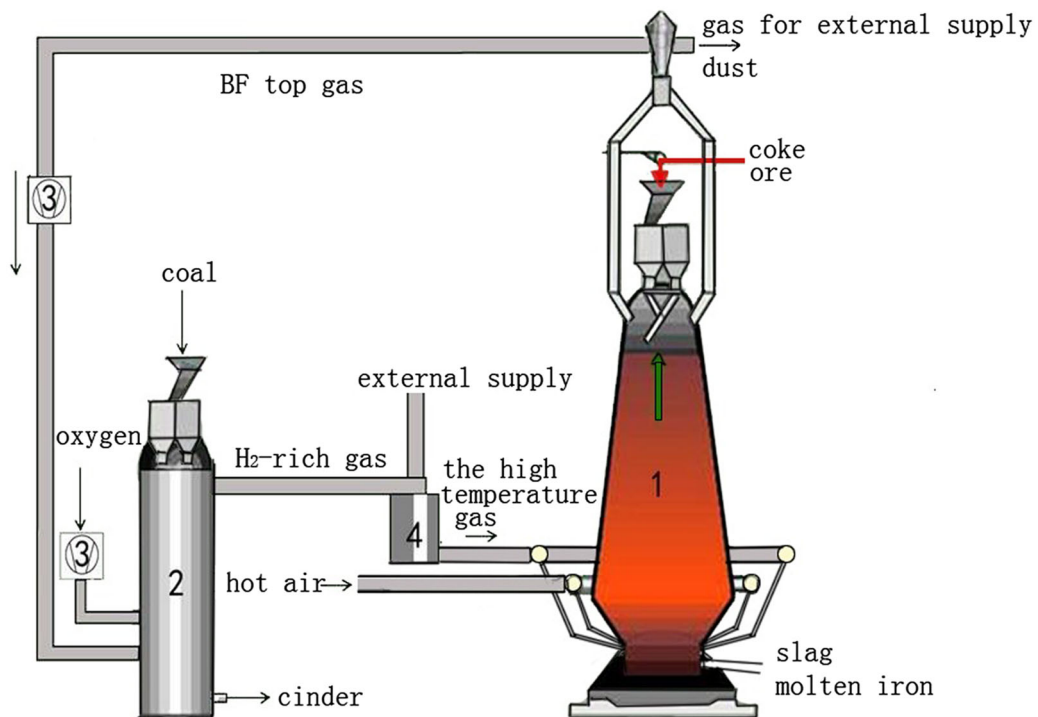


Fig. 1—Diagram describing the operation of the gas-injection BF. (1) Blast furnace, (2) gasifier, (3) pressure device, and (4) gas heating device.

this work, the tested specimens consisted of the industrially manufactured pellets with diameters of 12.0 to 16.0 mm and coke particles with diameters of 10.0 to 15.0 mm (their chemical compositions are listed in Tables I and II, respectively).

The schematic layout of the utilized experimental apparatus, which is capable of continuously evaluating the high-temperature properties of ferrous burden (including the shrinkage of the packed bed and pressure loss), is shown in Figure 2. It consists of an electric furnace, a temperature control system, a graphite crucible, a gas control system, a displacement meter, a loading apparatus, and auxiliary equipment. The rated power and highest heating temperature were equal to 12 kW and 1600 °C, respectively. The size of the graphite crucible was  $\varnothing 50$  mm  $\times$  140 mm. The ferrous burden, which has a layer thickness of 50 mm, was charged into a crucible, and 20 g of coke with a 20-mm layer thickness was placed above and below. The load applied during testing was 9.8 N/cm<sup>2</sup>.

The samples were heated at a rate of 10 °C/min below 1300 °C and at a rate of 5 °C/min above 1300 °C. The flow rate of N<sub>2</sub> gas (below 500 °C) was 5 L/min, and rate of the reducing gases (above 500 °C) was 15 L/min (see Table III). The reducing gases were supplied using high-pressure gas cylinders. The experiment was stopped after detecting the first drip of iron ore from the graphite crucible, which was followed by replacing the reducing gases with nitrogen and cooling the samples to room temperature. In addition, in order to detail the softening and melting process, some softening–melting tests were carried to completion, but many tests were terminated upon reaching different temperatures. The system was maintained at that temperature for 20 minutes to minimize the temperature difference between the samples and electric furnace. Then, the reducing gases were replaced by nitrogen before cooling the samples to room temperature.

### III. RESULTS AND DISCUSSION

#### A. Effect of H<sub>2</sub> Addition on the Softening Behavior of Ferrous Burden

H<sub>2</sub> addition has a strong influence on the softening and melting properties of ferrous burden, such as shrinkage (see Figure 3). As compared with the traditional BF (containing 30 pct CO without H<sub>2</sub>), the swelling of ferrous burden pellets at temperatures below 1000 °C was significantly decreased by the H<sub>2</sub> addition due to the improvement of their microstructure and reduction in pressure.<sup>[31–33]</sup>

After introducing H<sub>2</sub> gas into the gas-injection BF, the shrinkage of ferrous burden was initiated earlier than that in the traditional BF. To facilitate the comparison of the obtained test results, the softening behavior of the studied burden is often characterized by the  $T_{10 \text{ pct}}$  (the temperature, at which its volume shrinkage reaches 10 pct) and  $T_{40 \text{ pct}}$  (the temperature, at which the volume shrinkage reaches 40 pct) parameters, whereas the softening range corresponds to the interval between  $T_{10 \text{ pct}}$  and  $T_{40 \text{ pct}}$  ( $T_{40 \text{ pct}} - T_{10 \text{ pct}}$ ). A wider softening range is typically observed for the gas-injection BF with low initial softening and high finish temperatures. In this study, the initial softening temperatures measured at H<sub>2</sub> contents of 0, 5, 10, and 15 pct were 1185 °C, 1162 °C, 1124 °C, and 1145 °C, respectively. Furthermore, the positions of the shrinkage curves obtained at H<sub>2</sub> concentrations of 10 and 15 pct were very close to each other, indicating that changing the H<sub>2</sub> content from 0 to 10 pct produced a greater effect on the burden properties as compared to that observed after its increase from 10 to 15 pct. The reduction potential increases after H<sub>2</sub> addition, which enhances the formation of phases with low melting points (such as wüstite) and their solid solution below 1200 °C. The results of X-ray diffraction (XRD) analysis presented in Figure 4 show that the burden pellet before reduction is mainly composed of the hematite, magnesium ferrite oxide (MgFe<sub>2</sub>O<sub>4</sub>), and iron silicon oxide (Fe<sub>2.95</sub>Si<sub>0.05</sub>O<sub>4</sub>) phases. After increasing the H<sub>2</sub> content at a temperature of 1000 °C, the magnetite species are gradually replaced with wüstite and metallic iron (especially at H<sub>2</sub> concentrations greater than 10 pct). Hence, it was concluded that the reduction process from Fe<sub>2</sub>O<sub>3</sub> to Fe<sub>3</sub>O<sub>4</sub> could be shortened in gas-injection BF, and large amounts of FeO and metallic iron are generated at a lower temperature, thus decreasing the initial softening temperature and reducing the expansion during the reduction process.

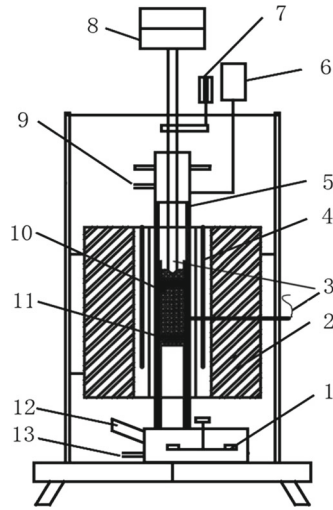
However, at temperatures above 1200 °C, the softening behavior of the ferrous burden pellets becomes mainly dependent on the thickness of their iron shells, as indicated by the results of previous studies.<sup>[34]</sup> Without an applied load, the profiles of the pellets reduced by the 30 pct CO + 0 pct H<sub>2</sub>, 30 pct CO + 5 pct H<sub>2</sub>, 30 pct CO + 10 pct H<sub>2</sub>, and 30 pct CO + 15 pct H<sub>2</sub> gas

**Table II. Chemical Composition and Properties of the Coke Used in this Study (Mass Percent)**

C	Volatile	Ash	S	CRI	CSR
85.71	1.60	12.20	0.49	25.16	67.31

**Table I. Chemical Compositions of the Ferrous Burden Pellets (Mass Percent)**

TFe (Total Fe)	Fe <sub>2</sub> O <sub>3</sub>	FeO	SiO <sub>2</sub>	CaO	MgO	Al <sub>2</sub> O <sub>3</sub>	TiO <sub>2</sub>	MnO	P <sub>2</sub> O <sub>5</sub>	Others
60.15	83.05	2.59	6.32	1.65	1.11	1.23	0.24	0.10	0.07	3.63



1 – drip receiver, 2 – electric furnace, 3 – thermocouples, 4 – silicon carbon tube, 5 – alundum tube, 6 – differential pressure gauge, 7 – displacement meter, 8 – loading apparatus, 9 – gas outlet, 10 – graphite pusher, 11 – graphite crucible, 12 – drip detector, 13 – gas inlet

Fig. 2—Experimental apparatus for evaluating the high-temperature properties of ferrous burden under loading.

**Table III. Compositions of the Reducing Gases Used in this Study (Volume Percent)**

	CO	H <sub>2</sub>	N <sub>2</sub>
1#	30	0	70
2#	30	5	65
3#	30	10	60
4#	30	15	55

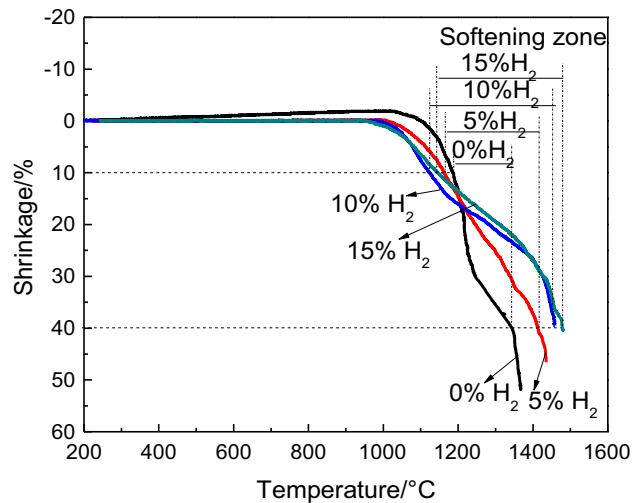


Fig. 3—Effect of H<sub>2</sub> addition on the shrinkage of ferrous burden pellets at elevated temperatures.

mixtures exhibit significant differences at 1300 °C, as shown in Figure 5. The specimen treated with the 30 pct CO + 0 pct H<sub>2</sub> mixture contains a dark wüstite core

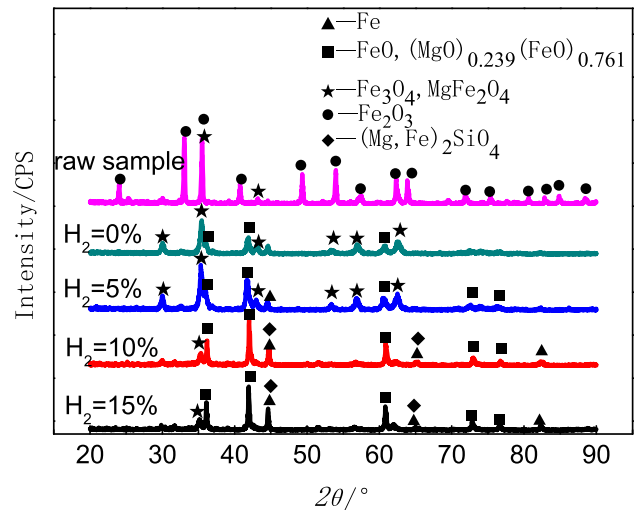


Fig. 4—XRD patterns of the pellets cooled from 1000 °C at different H<sub>2</sub> contents.

surrounded by a thin rim of metallic iron (this wüstite core is different from the wüstite phase obtained at lower temperatures since it is granular and precipitated from the melt, which will be discussed in more detail in the subsequent sections<sup>[35]</sup>). As the liquid volume fraction increases with increasing temperature, the mechanical strength of the core decreases, and its resistance to deformation is mainly determined by the properties of the iron shell.<sup>[34]</sup> With increasing the H<sub>2</sub> concentration in the reducing mixture, the thickness of the iron shell increases, while the volume of the wüstite core gradually decreases and finally disappears altogether at an H<sub>2</sub> content of 15 pct (Figure 5). Thus, the

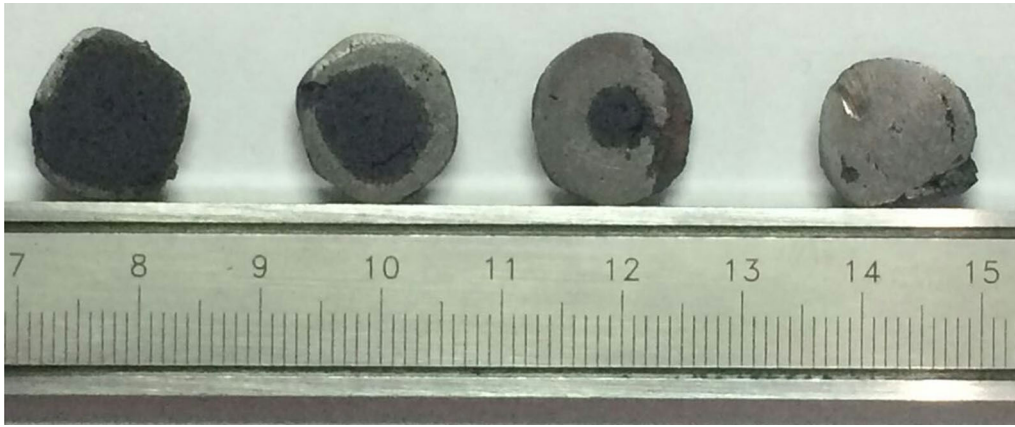


Fig. 5—Cross-sections of the burden pellets cooled from 1300 °C in the experiments with H<sub>2</sub> contents of (from left to right) 0, 5, 10, and 15 pct.

thicker iron shell exhibits higher resistance to deformation, which increases the softening finish temperature and widens the softening range.

### B. Effect of H<sub>2</sub> Addition on the Dripping Behavior of Ferrous Burden

To characterize the melting behavior of ferrous burden, its initial melting temperature ( $T_s$ ) and dripping temperature ( $T_d$ ) were measured (the melting range was determined from the interval between  $T_s$  and  $T_d$  ( $\Delta T_{ds} = T_d - T_s$ )). Here  $T_s$  is defined as the temperature corresponding to a significant jump in the differential pressure, whereas  $T_d$  represents a temperature, at which the melt receiver collects the first drip from the graphite crucible. The results presented in Figure 6 reveal that H<sub>2</sub> addition strongly affects the burden dripping behavior. The values of both  $T_s$  and  $T_d$  increase with increasing H<sub>2</sub> content, leading to a decrease in the melting interval (especially at H<sub>2</sub> concentrations greater than 10 pct), which produces a significant effect on the ameliorating permeability of the BF.

It is well known that the magnitude of  $T_s$  is related to the parameters of the formed slag and burden, such as the solidus temperature, fluidity of melt, pore structure, reduction degree, and compositions of the constituent mineral phases.<sup>[36]</sup> During the treatment with the 30 pct CO + 0 pct H<sub>2</sub> gas mixture, the reduction process is significantly inhibited at a temperature of around 1200 °C, leading to the decrease in porosity caused by the diffusion of the melt into fine pores (the corresponding solidus temperature is equal to 1180 °C, *i.e.*, the eutectic of FeO-2FeO-SiO<sub>2</sub> in SiO<sub>2</sub>-CaO-FeO slag<sup>[37]</sup>). At 1218 °C, the wüstite core begins to flow abruptly under loading and capillary force<sup>[22]</sup>; as a result, the differential pressure increases continuously, and melting reduction occurs. The reduction degree and thickness of the iron shell of the burden pellet increase with H<sub>2</sub> addition, while the amount of FeO decreases, which increases  $T_s$  because the melting point of metallic iron is higher than that of FeO. The composition of the slag obtained *via* chemical analysis is displayed in Figure 7,<sup>[38]</sup> which shows that the fraction of the phases

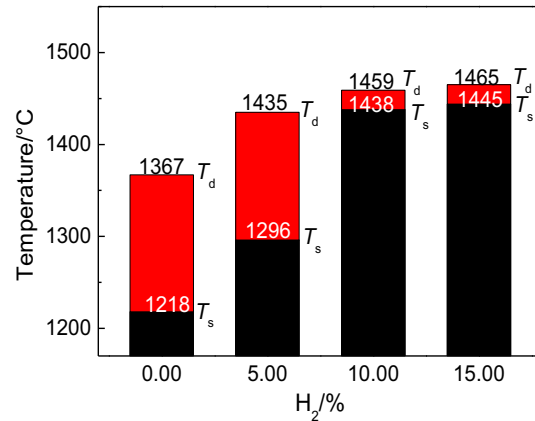


Fig. 6—Influence of H<sub>2</sub> addition on the melting zone distribution in the gas-injection BF.

with high-melting points gradually increases with increasing H<sub>2</sub> content, except for the 30 pct CO + 5 pct H<sub>2</sub> mixture because the composition of point B primarily corresponds to fayalite crystals. However, the amount of the melt significantly decreases at larger H<sub>2</sub> concentrations. As mentioned above, with the increasing H<sub>2</sub> content, the initial melting temperature ( $T_s$ ) is observed to increase, accompanied by increases in the reduction degree, thickness of iron shell, and amount of the high-melting point phases. Moreover, for the ternary CaO-SiO<sub>2</sub>-FeO system,<sup>[38]</sup> the tendency for increasing  $T_s$  at a higher reduction potential in the gas-injection BF persists, despite the wide basicity range of the burden structure.

On the other hand, the dripping temperature ( $T_d$ ) of the ferrous burden is strongly affected by the carburization of iron and concentration of the molten iron phase.<sup>[36]</sup> The carburization of metallic iron mainly involves the following two processes: the carburization of metallic iron by CO in the lumpy section and carburization by coke in the melting zone. Although the H<sub>2</sub> addition enhances the former process, the dripping behavior of ferrous burden mainly depends on the second factor.<sup>[39,40]</sup> During the treatment with the 30 pct CO + 0 pct H<sub>2</sub> mixture at a temperature above

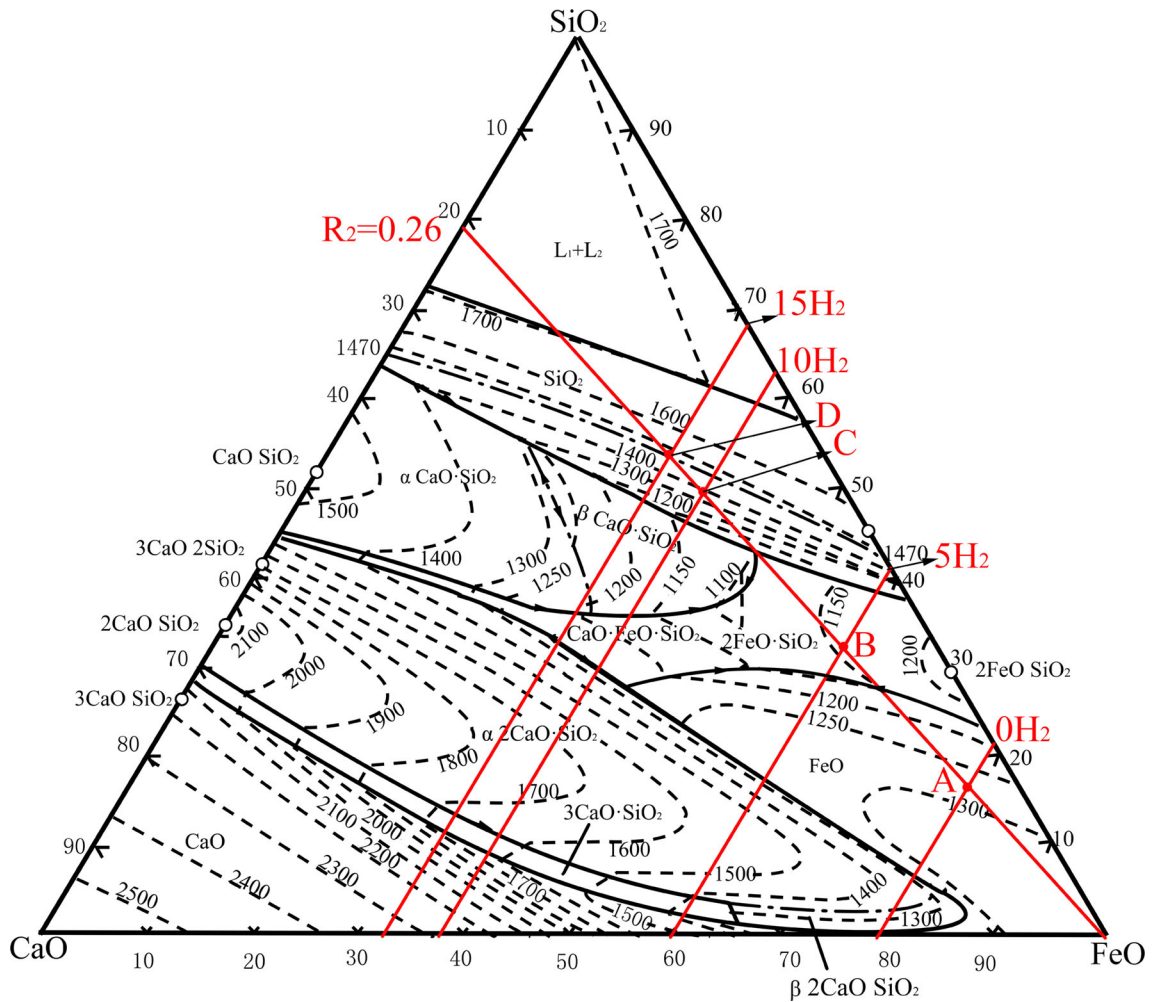


Fig. 7—Slag composition with different H<sub>2</sub> contents at 1300 °C in the CaO-SiO<sub>2</sub>-FeO ternary phase diagrams. Adapted from Ref. [38].

1218 °C, the exudation of the liquid slag promotes the cementation process by increasing the contact area between the iron metal and the coke.<sup>[22]</sup> However, this physical contact is limited by the lower amounts of liquid oxides and solid phase formed after H<sub>2</sub> addition, which increases the dripping temperature. Figure 8 shows the mineralogical structures of the pellets treated with different H<sub>2</sub> contents without a load. Within the periphery of the pellet, the metallic iron becomes immersed in the liquid fayalite and deformable wüstite phases after the treatment with the 30 pct CO + 0 pct H<sub>2</sub> mixture at 1300 °C, which decreases the strength of the solid structure and reduction rate. The metallic iron on the external surface is present as a dense rim and is considerably finer than that in the interior (the top right corner of Figure 8(a)). However, several tiny metallic iron particles are scattered among the abundant molten granular wüstite species in the pellet center, which precipitated from the melt.<sup>[35]</sup> In contrast, at an H<sub>2</sub> concentration of 5 pct, the molten wüstite and fayalite are replaced by a considerably greater number of pores and a spot of silicate glass in both the pellet periphery and center with the decrease of melt, which improves the high-temperature reduction properties. When the H<sub>2</sub>

content exceeds 10 pct (in particular, at a magnitude of 15 pct), the Wüstite-containing molten slag phase disappeared in the pellet center. The structure consisting of metallic iron and silicate melt gradually occupies the entire pellet followed by the sintering of metallic iron particles into coarse grains. Without the exudation of the molten wüstite from the center of the pellet, the pellets retain their original shape until reaching higher temperatures, which does not favor the contact of liquid oxides with coke and increases the dripping temperature ( $T_d$ ). This fact implies that the reduction rate is much faster than the carburization rate with H<sub>2</sub> addition, and the carburization determines the dripping behavior of ferrous burden in the gas-injection BF with a high reduction potential. These results are consistent with the carbon contents in the metallic iron phase at the pellet peripheries (Table IV) obtained *via* electron probe microanalysis (EPMA). Thus, the carbon content in metallic iron apparently decreases with H<sub>2</sub> addition, especially at H<sub>2</sub> contents greater than 10 pct.

Accordingly, during H<sub>2</sub> addition, once Fe-C melt is formed in the higher-temperature zone adjacent to the carbon source (where the cohesion of metal iron particles is not impeded by the presence of slag), its

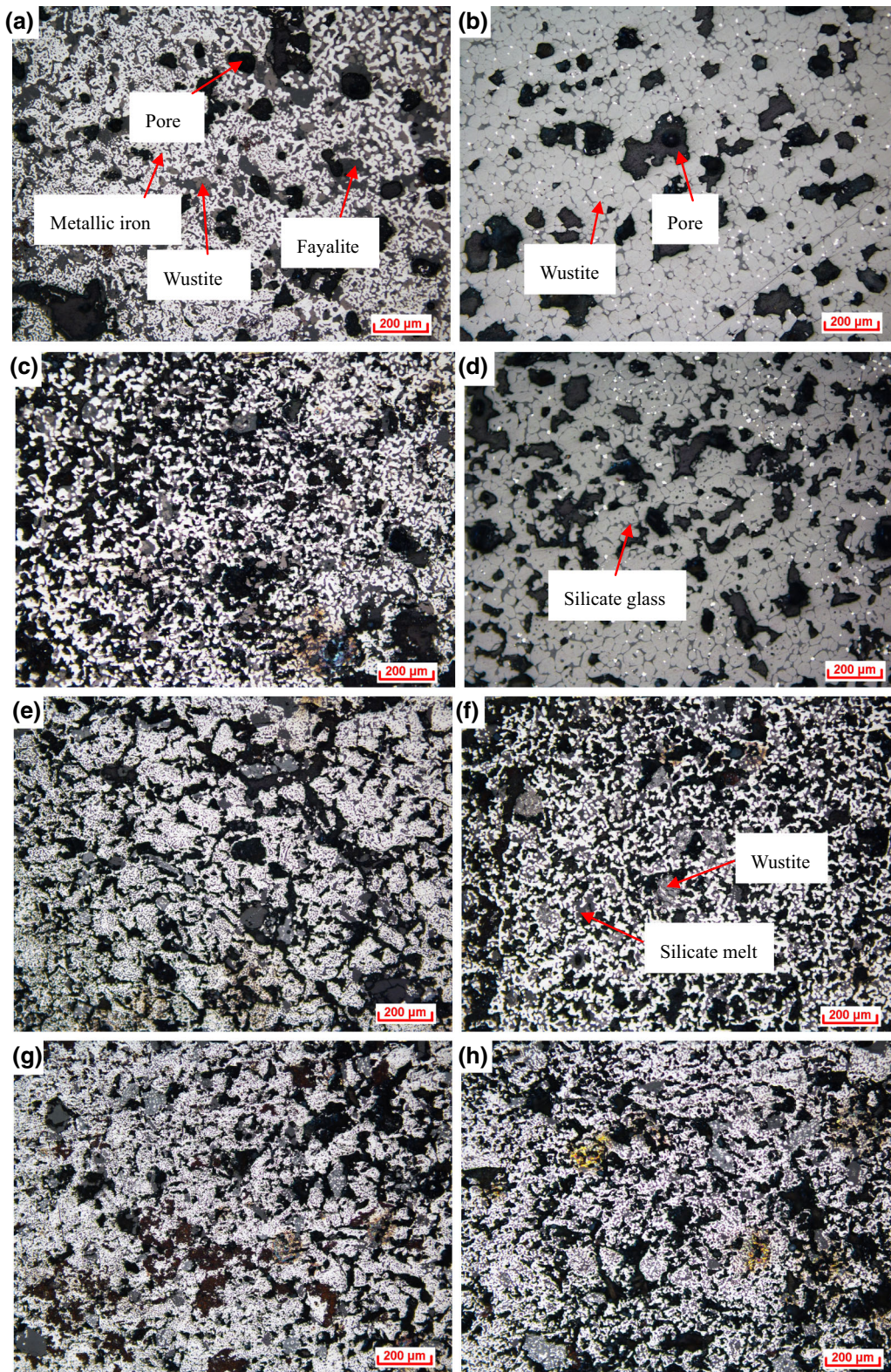


Fig. 8—Mineralogical structures of pellets cooled from 1300 °C after reduction with different H<sub>2</sub> contents (optical microscopy). (a) Periphery and (b) center of the pellet treated with 30 pct CO + 0 pct H<sub>2</sub>; (c) periphery and (d) center of the pellet treated with 30 pct CO + 5 pct H<sub>2</sub>; (e) periphery and (f) center of the pellet treated with 30 pct CO + 10 pct H<sub>2</sub>; and (g) periphery and (h) center of the pellet treated with 30 pct CO + 15 pct H<sub>2</sub>.

carburization rapidly occurs leading to meltdown. Figure 9 displays the XRD patterns of the residue after samples dripping from the graphite crucible. They show

the presence of a large amount of unreduced iron oxide and fayalite in the molten slag after the treatment with the 30 pct CO + 0 pct H<sub>2</sub> mixture; however, a broad

peak in the diffraction pattern suggested that only some amorphous phase (*i.e.*, silicate melt for acidic pellets) remained in the molten slag after H<sub>2</sub> addition, indicating that H<sub>2</sub> treatment is effective in separating molten iron and slag in the gas-injection BF.

### C. Effect of H<sub>2</sub> Addition on the Permeability of a Stock Column

The *S* value (corresponding to the cumulative pressure drop in a BF) is used for evaluating the permeability of a stock column during reduction.<sup>[36]</sup> Its magnitude can be calculated by integrating the pressure drop over temperature *via* the formula  $S = \int_{T_s}^{T_d} (\Delta P_{\max} - \Delta P_s) dT$ . Here  $\Delta P_{\max}$  is the maximum pressure difference, and  $\Delta P_s$  is the pressure drop at  $T_s$ . Figure 10 shows the gas permeability indexes determined at various experimental conditions. As was discussed previously in Section III–B, the continuous increase in the differential pressure observed during the treatment with the 30 pct CO + 0 pct H<sub>2</sub> mixture is attributed to the exudation of the liquid phase from the wüstite core. However, the resulting melts exhibit high viscosity and poor fluidity at the  $T_s$ ,<sup>[25]</sup> which results in a relatively high value of pressure loss and subsequent meltdown (see Figure 10(a)). For comparison, after the temperature reaches the  $T_s$ , the pressure loss increases intensely during the treatment with the 30 pct

**Table IV. EPMA Analysis of the Pellet Peripheries Treated at Various H<sub>2</sub> Contents (Mass Percent)**

Atmosphere	Carbon Content in Metallic Iron
30 pct CO + 0 pct H <sub>2</sub>	2.6
30 pct CO + 5 pct H <sub>2</sub>	1.2
30 pct CO + 10 pct H <sub>2</sub>	0.9
30 pct CO + 15 pct H <sub>2</sub>	0.8

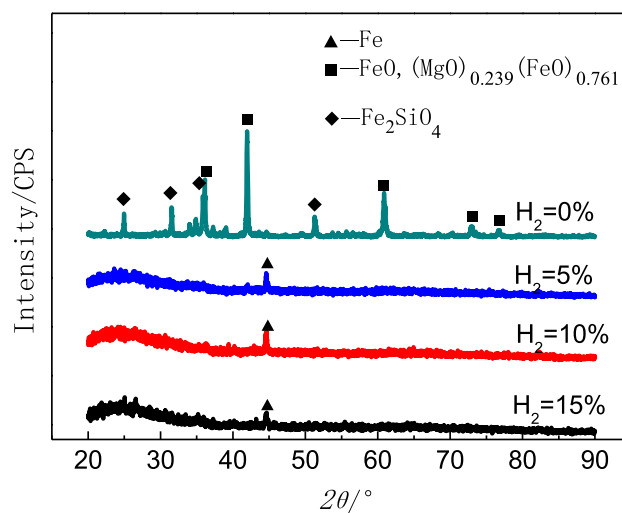


Fig. 9—XRD patterns of the ferrous burden samples recorded before and after H<sub>2</sub> treatment (residue after dripping).

CO + 5 pct H<sub>2</sub> mixture; however, this process does not last long due to the fluidity enhancement that occurs at high temperatures. When the H<sub>2</sub> content exceeds 10 pct, the *S* value and  $\Delta P_{\max}$  decrease sharply owing to the formation of a smaller amount of liquid oxides and a higher number of porous metallic iron grains, which is consistent with the results presented in Figure 8. The values of  $\Delta P_{\max}$  obtained at the four different concentrations of H<sub>2</sub> utilized in this study are equal to 21.9, 14.49, 0.72, and 0.88 kPa, while the corresponding *S* values amount to 1163, 786, 19, and 12 kPa °C, respectively. From these results, it can be concluded that the observed enhancement of the softening–melting behavior in the gas-injection BF with H<sub>2</sub> addition is related to the higher reduction degree and the decreased amount of FeO in the melt.

In addition, the *S* value is strongly dependent on the melt amount in the melting zone. The quantity of liquid phase was estimated using thermodynamic calculations on the CaO–SiO<sub>2</sub>–Al<sub>2</sub>O<sub>3</sub>–MgO–FeO system including all gangue and unreduced FeO. For simplicity, it was assumed that the masses of the Al<sub>2</sub>O<sub>3</sub> and MgO phases were equivalent to those of the SiO<sub>2</sub> and CaO ones, respectively.<sup>[25]</sup> The mass fraction of the liquid phase was obtained from the isothermal phase diagram of the CaO–SiO<sub>2</sub>–FeO system (Figure 11), which was constructed using FactSage 7.0 software. If the postulated mass of the CaO–SiO<sub>2</sub>–FeO phase after the treatment with the 30 pct CO + 0 pct H<sub>2</sub> mixture at 1300 °C is 100 kg, the mass of the CaO–SiO<sub>2</sub>–FeO mixture after the H<sub>2</sub> addition at concentrations of 5, 10, and 15 pct (estimated from the material balance from the results of exhaust gas and the quality of reduced iron analysis) are equal to 65.87, 32.26, and 29.41 kg, respectively. Clearly, the chemical compositions of points A and B are fully within the liquid region at 1300 °C. The compositions of the other two points are located in the area containing tridymite crystals, and their liquid fractions were calculated according to the lever rule. The obtained results show that after the addition of 5, 10, and 15 pct H<sub>2</sub>, the amounts of the produced melt correspond to 65.87, 31.31, and 27.01 pct of the mass obtained after the treatment with the 30 pct CO + 0 pct H<sub>2</sub> mixture, respectively, suggesting that the content of the liquid slag decreases significantly after H<sub>2</sub> addition to the gas-injection BF.

$$m_{C(L)} = \frac{CE}{C_1E} m_C = \frac{49.5}{51.0} \times 32.26 \text{ kg} = 31.31 \text{ kg}$$

$$m_{D(L)} = \frac{DE}{D_1E} m_D = \frac{45}{49} \times 29.41 \text{ kg} = 27.01 \text{ kg}$$

Furthermore, as described above, the large amounts of liquid oxides exuded in the traditional BF not only block the gas channels and increase the pressure drop but also react with the carbon species in the adjacent coke zone, causing either a direct reduction reaction or melting reduction. Compared with melting reduction, reduction using reducing gases consumes less energy. Owing to the high reduction potential, the iron oxide species were almost fully reduced to metallic iron before the temperature reached the  $T_s$  value, which improved



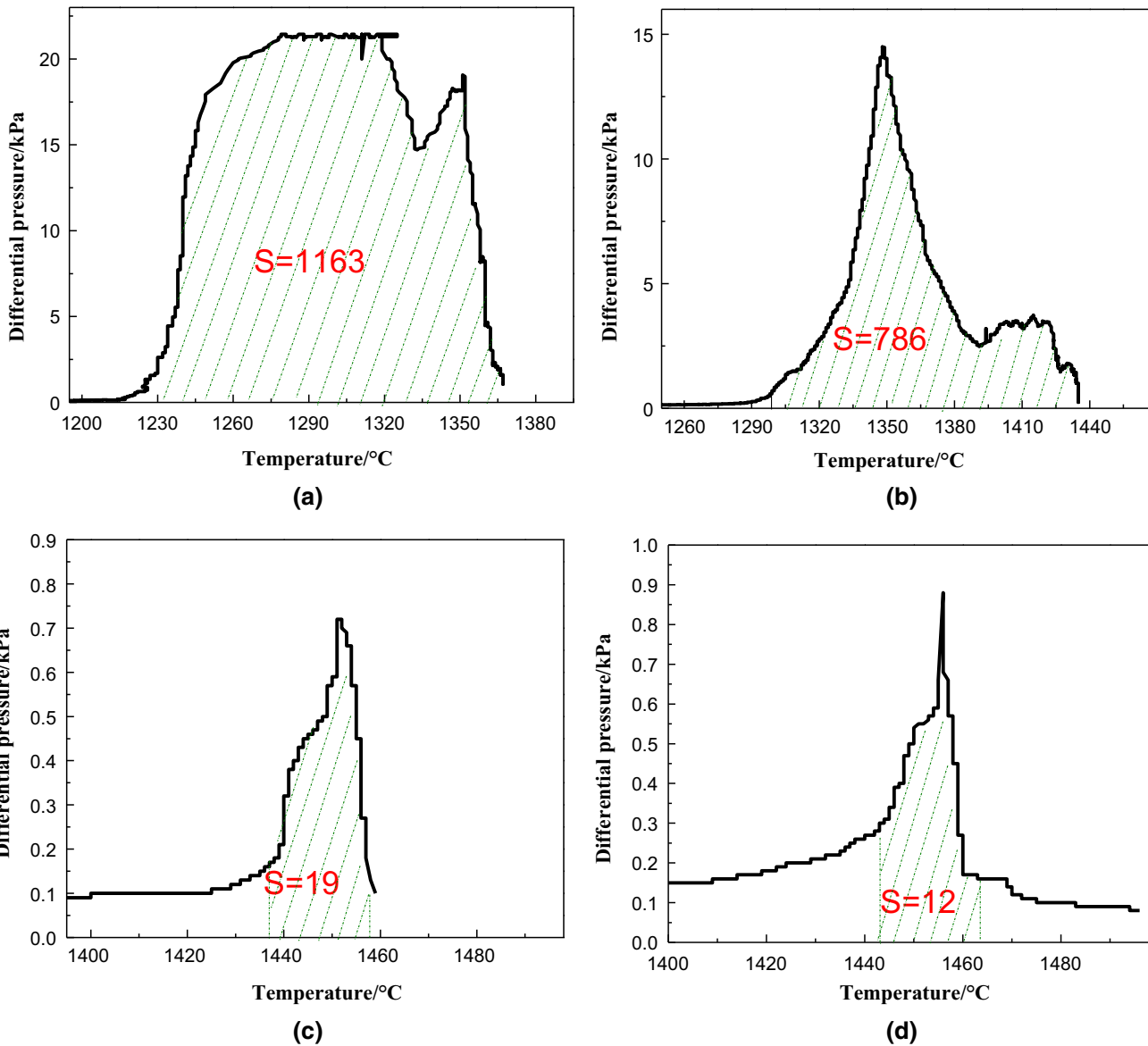


Fig. 10—Gas permeability indexes measured at different H<sub>2</sub> contents. (a) 30 pct CO + 0 pct H<sub>2</sub>, (b) 30 pct CO + 5 pct H<sub>2</sub>, (c) 30 pct CO + 10 pct H<sub>2</sub>, and (d) 30 pct CO + 15 pct H<sub>2</sub>.

the softening and melting properties of ferrous burden, narrowed the melting zone, enhanced the bed permeability, and lowered the fuel ratio in the gas-injection BF.

#### D. Optimum H<sub>2</sub> Content in the Gas-Injection BF

Using the above-mentioned procedure, the positions of the softening and melting zones with different H<sub>2</sub> contents were obtained (see Figure 12). It should be noted that the two parameters concerning the melt forming properties, *i.e.*, the softening finishing temperature ( $T_{40 \text{ pct}}$ ) and initial melting temperature ( $T_s$ ), are not mutually exclusive because they are evaluated from different perspectives.<sup>[41,42]</sup> As shown in Figure 12, in contrast to the rapid increase in  $T_s$  and  $T_d$ , the value of  $T_{10 \text{ pct}}$  is slightly lowered with increasing H<sub>2</sub> content.

The softening zone becomes wider; however, the width of the melting zone, which represents the main parameter affecting the bed permeability, decreases and ultimately approaches zero. Furthermore, lowering the position of the cohesive zone in the gas-injection BF and minimizing its size both improve the furnace productivity and decrease the coke rate.

In addition, it should be noted that the effects of H<sub>2</sub> addition on the softening and melting reduction behaviors were not very pronounced when the H<sub>2</sub> content was increased from 10 to 15 pct, as compared to the effects of increasing the H<sub>2</sub> contents from 0 to 10 pct. The results of previous studies indicate that an excessively high reduction potential can decrease the amount of iron oxides in the lumpy section, leading to a poorer distribution of energy and lower gas utilization efficiency.<sup>[43,44]</sup> According to the data obtained in this

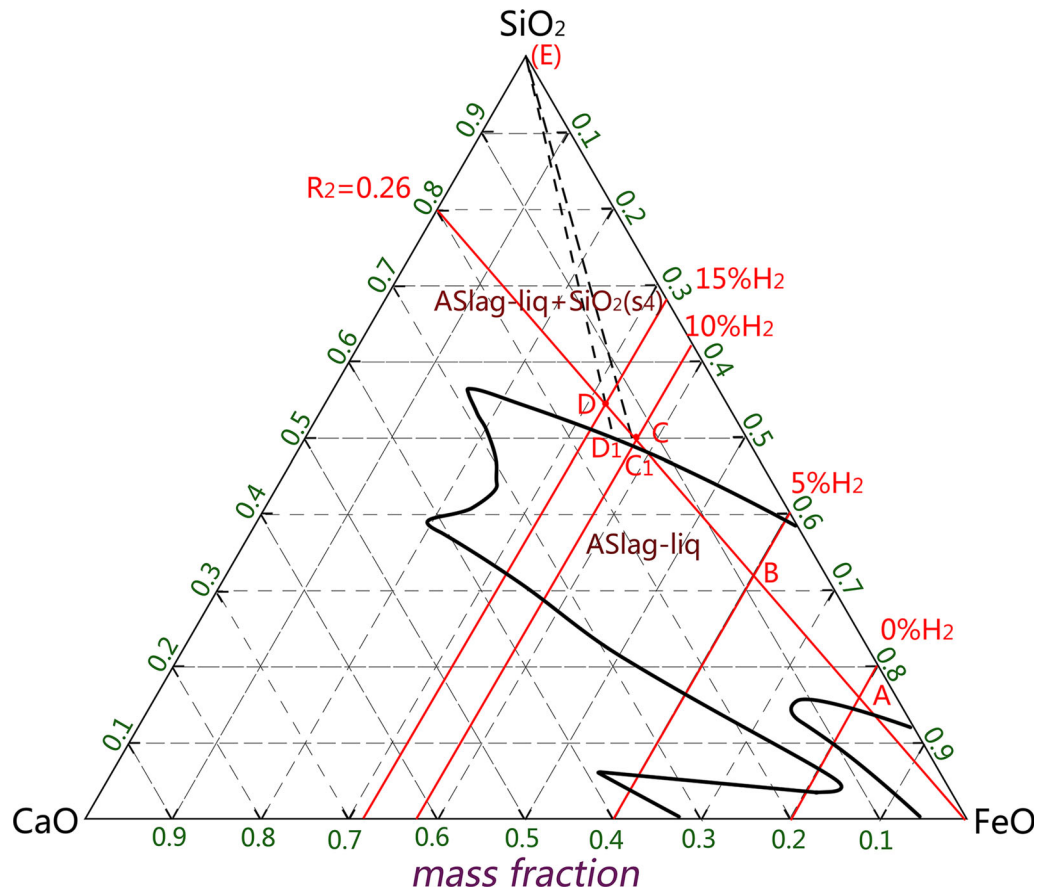


Fig. 11—Isothermal phase diagram constructed using FactSage 7.0 for the CaO-SiO<sub>2</sub>-FeO system at a temperature of 1300 °C.

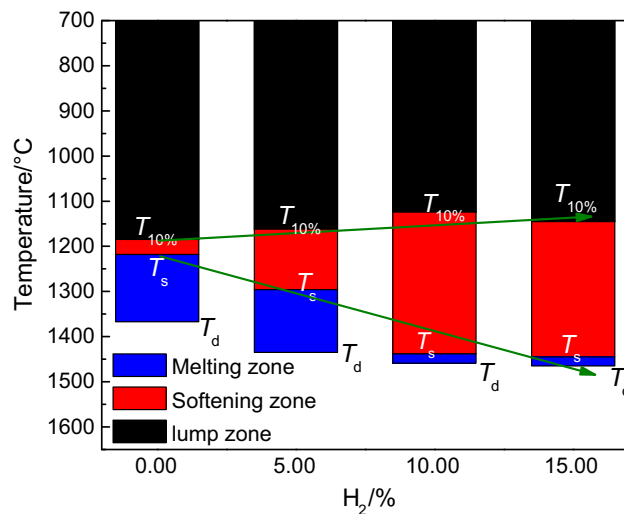


Fig. 12—Influence of H<sub>2</sub> addition on the distributions of the softening and melting zones in the gas-injection BF.

work, the process occurring inside the gas-injection BF is characterized by a relatively high softening finish temperature, narrow range of the melting temperature, and good permeability of the gas phase, which meet the requirements for the next-generation BF. After considering the effects of H<sub>2</sub> addition on the reduction rate,

amount of the produced melt, burden microstructure, and energy consumption efficiency of the gas-injection BF, the optimal H<sub>2</sub> content can be concluded to lie between 10 and 15 pct.

#### IV. CONCLUSIONS

As compared to the traditional BF, the gas-injection BF with H<sub>2</sub> gas flow is characterized by a higher reduction rate, lower amount of the primary slag, and greater bed permeability as well as a smaller size of the cohesive zone in a lower position. Overall, from synthetic consideration of the effect of H<sub>2</sub> addition on the reduction rate, amount of the melt, burden microstructure, and energy efficiency in the gas-injection BF, it was found that optimal H<sub>2</sub> content lied between 10 and 15 pct. From the obtained results, the following conclusions have been drawn.

1. The improvement of the transformation rate of Fe<sub>2</sub>O<sub>3</sub> to Fe<sub>3</sub>O<sub>4</sub> due to H<sub>2</sub> addition generates large amounts of FeO and metallic iron at relatively low temperatures, which reduces the swelling of burden pellets below 1000 °C. The initial softening temperature decreases with increasing H<sub>2</sub> concentration, while the softening finish temperature increases due to the thicker iron shell and lower amount of residual FeO.

2. The initial melting and dripping temperatures increase with increasing H<sub>2</sub> concentration, which significantly narrows the melting interval (especially at H<sub>2</sub> contents greater than 10 pct). In addition, the carburization determines the dripping behavior of the ferrous burden in the gas-injection BF with a high reduction potential.
3. The stock column permeability is improved because of the lower melt quantity in the cohesive zone; this is because the iron oxides are almost reduced to metallic iron with high reduction potential in gas-injection BF.
4. In contrast to the increase in the H<sub>2</sub> content from 5 to 10 pct, a relatively modest improvement in the high-temperature properties of the ferrous burden (including its softening behavior, dripping behavior, and permeability index) was observed after further increasing the H<sub>2</sub> concentration from 10 to 15 pct.

### ACKNOWLEDGMENTS

This work was performed in the Key Laboratory for Advanced Metallurgy Technology of the North China University of Science and Technology. The authors are grateful for the support provided through the Key Program of the National Nature Science Foundation of China (Grant No. U1360205), Graduate Student Innovation Fund of North China University of Science Technology (Grant No. 2015B01), and North China University of Science and Technology Distinguished Youth Scholars Fund (Grant No. JP201508).

### REFERENCES

1. World Steel Association (Belgium, Brussels): <https://www.worldsteel.org/zh/media-centre/press-releases/2015/the-steel-industry-calls-for-a-reinforced-partnership.html>, 2015. Assessed 29 July 2015.
2. K.D. Xu: *Iron Steel*, 2010, vol. 45, pp. 1–12.
3. E.P. da Rocha, V.S. Guiherme, J.A. de Castro, Y. Sasaki, and J. Yagi: *J. Mater. Res. Technol.*, 2013, vol. 2, pp. 255–62.
4. K.S. Abdel Halim: *J. Iron. Steel Res. Int.*, 2013, vol. 20, pp. 40–46.
5. M.S. Chu, H. Nogami, and J.I. Yagi: *ISIJ Int.*, 2004, vol. 44, pp. 801–08.
6. O. Lingiardi, O. Burrai, C.G. Fuentealba, P. Etchevarne, and J.M. Gonzalez: *ICSTI/Ironmaking Conference Proceedings*, ISS, Warrendale, PA, 1998, vol. 57, p. 135.
7. J.M. Steer, R. Marsh, M. Greenslade, and A. Robinson: *Fuel*, 2015, vol. 151, pp. 40–49.
8. S.W. Du, C.P. Yeh, W.H. Chen, C.H. Tsai, and J.A. Lucas: *Fuel*, 2015, vol. 143, pp. 98–106.
9. V. Trinkel, N. Kieberger, T. Bürgler, H. Rechberger, and J. Fellner: *J. Clean. Prod.*, 2015, vol. 94, pp. 312–20.
10. C. Wanga, M. Larsson, J. Lövgren, P. Mellin, W. Yang, H. Salman, and A. Hultgren: *Energy Procedia*, 2014, vol. 61, pp. 2184–87.
11. W.H. Chen, C.L. Hsu, and S.W. Du: *Energy*, 2015, vol. 86, pp. 758–71.
12. W.H. Chen, M.R. Lin, A.B. Yu, S.W. Du, and T.S. Leu: *Int. J. Hydrogen Energy*, 2012, vol. 37, pp. 11748–58.
13. H. Ghanbari, F. Pettersson, and H. Saxén: *Chem. Eng. Sci.*, 2015, vol. 129, pp. 208–22.
14. P. Jin, Z. Jiang, C. Bao, S. Hao, and X. Zhang: *Resour. Conserv. Recycl.*, 2015, vol. 3062, pp. 1–3.
15. G. Danloy, A. Berthelemot, M. Grant, and J. Borlee: *Rev. Metall.*, 2009, vol. 106, pp. 1–8.
16. L. Hooley, A. Tobiesen, J. Johns, and S. Santos: *Energy Procedia*, 2013, vol. 37, pp. 7139–51.
17. R. Schott: *Iron Steel Technol.*, 2013, vol. 3, pp. 63–75.
18. H.B. Luengen, M. Peters, and P. Schmöle: *Iron Steel Technol.*, 2012, vol. 9, pp. 63–76.
19. Q. Lyu, F.M. Li, and X.B. Li: *Iron Steel*, 2008, vol. 43, pp. 17–21.
20. F.M. Li, Q. Lyu, and X.B. Li: *Iron Steel*, 2007, vol. 42, pp. 12–15.
21. H. Guo, F.M. Li, and Q. Lyu: *J. Hebei Inst. Technol.*, 2007, vol. 29, pp. 27–31.
22. I. Shigaki, S. Shirouchi, K. Tokutake, and N. Hasegawa: *ISIJ Int.*, 1990, vol. 30, pp. 199–207.
23. P.F. Nogueira and R.J. Fruehan: *Metall. Mater. Trans. B*, 2004, vol. 35B, pp. 829–38.
24. P.F. Nogueira and R.J. Fruehan: *Metall. Mater. Trans. B*, 2005, vol. 35B, pp. 583–90.
25. T. Nishimura, K. Higuchi, M. Naito, and K. Kunitomo: *ISIJ Int.*, 2011, vol. 51, pp. 1316–21.
26. K. Sunahara, T. Natsui, K. Shizawa, and Y. Ujisawa: *ISIJ Int.*, 2011, vol. 51, pp. 1322–32.
27. M. Matsumura, M. Hoshi, and T. Kawaguchi: *ISIJ Int.*, 2005, vol. 45, pp. 594–602.
28. X.W. An, J.S. Wang, R.Z. Lan, Y.H. Han, and Q.G. Xue: *J. Iron. Steel Res. Int.*, 2013, vol. 20, pp. 11–16.
29. H.J. Zhang, X.F. She, Y.H. Hua, J.S. Wang, F.B. Zeng, and Q.G. Xue: *J. Iron. Steel Res. Int.*, 2015, vol. 22, pp. 297–303.
30. W.J. Yang, Z.Y. Zhou, A.B. Yu, and D. Pinson: *Powder Technol.*, 2015, vol. 279, pp. 134–45.
31. Z.K. Liang: Master thesis, Central South University, Changsha, China, 2013.
32. Z.C. Wang: Master thesis, Northeastern University, Shenyang, China, 2009.
33. L.Y. Yi: PhD thesis, Central South University, Changsha, China, 2013.
34. T. Bakker: PhD thesis, Delft University of Technology, Delft, Netherlands, 1999.
35. C.E. Loo, L.T. Matthews, and D.P. O’Dea: *ISIJ Int.*, 2011, vol. 51, pp. 930–38.
36. K. Higuchi, M. Naito, M. Nakano, and Y. Takamoto: *ISIJ Int.*, 2004, vol. 44, pp. 2057–66.
37. X.H. Huang: *Principles of Steel Metallurgy*, 3rd ed., Press of Metallurgy Industry, Beijing, 2010, p. 140.
38. X.H. Huang: *Principles of Steel Metallurgy*, 3rd ed., Press of Metallurgy Industry, Beijing, 2010, p. 160.
39. Y. Iguchi and S. Endo: *ISIJ Int.*, 2004, vol. 44, pp. 1991–98.
40. G.Y. Ren: *Ironmaking*, Press of Metallurgical Industry, Beijing, 2008, pp. 239–41.
41. J.X. Liu, G.J. Cheng, Z.G. Liu, M.S. Chu, and X.X. Xue: *Int. J. Miner. Process.*, 2015, vol. 142, pp. 113–18.
42. K. Higuchi, Y. Takamoto, T. Orimoto, T. Sato, F. Koizumi, K. Shinagawa, and H. Furuta: *Nippon Steel Techn. Rep.*, 2006, vol. 94, pp. 36–41.
43. Y.N. Qie, Q. Lyu, J.P. Li, C.C. Lan, and X.J. Liu: *ISIJ Int.*, 2017, vol. 57, pp. 404–12.
44. Q. Lyu, Y.N. Qie, X.J. Liu, C.C. Lan, J.P. Li, and S. Liu: *Thermochim. Acta*, 2017, vol. 648, pp. 79–90.